Distribution and stability of Mn complexes in the ocean: Influence of hydrothermal plumes and weather events

Aubin Thibault de Chanvalon, George Luther, Véronique Oldham, Bradley Tebo, Nicole Coffey, Timothy Shaw

Distribution and stability of Mn complexes in the ocean: influence of hydrothermal plumes and weather events.

Aubin Thibault de Chanvalon[1,2]*, aubin.thibault-de-chanvalon@univ-pau.fr [1]University of Delaware School of Marine Science & Policy, 700 Pilottown Road, Lewes, DE, 19958, USA [2]CNRS, Universite de Pau et des Pays de l'Adour, E2S UPPA, IPREM, UMR 5254, Pau, France

George W. Luther III[1], luther@udel.edu [1]University of Delaware School of Marine Science & Policy, 700 Pilottown Road, Lewes, DE, 19958, USA

Véronique E. Oldham[1,3], voldham@uri.edu [1]University of Delaware College of Earth, Ocean, and Environment, 700 Pilottown Road, Lewes, DE, 19958, USA, [3]University of Rhode Island, Graduate School of Oceanography, 215 S Ferry Lane, Narragansett, RI, 02882, USA

Bradley M. Tebo[4], tebob@ohsu.edu, [4]Oregon Health & Science University, Portland, OR, 97239, USA. Current address: University of Washington, Seattle, WA 98195

Nicole R. Coffey[1,6], coffeyni@oregonstate.edu, [6]Oregon State University, College of Earth, Ocean, and Atmospheric Sciences, Corvallis, OR, 97331-4501, USA

Timothy F. Shaw[5], SHAW@mailbox.sc.edu, [5]University of South Carolina, Columbia, SC, 29208, USA

Key words: Manganese; metal speciation; Oxygen minimum zone; biogeochemistry; hydrothermal plume; complexes stability;

Running head: Stability of Mn complexes in ocean

Abstract

We measured the speciation of dissolved Mn from the surface to just above the hydrothermal vents at 9°50'N East Pacific Rise in the open ocean of the Pacific over a three week period. Total dissolved Mn concentrations ranged from 2.2 to 135 nM with a significant contribution of dissolved Mn(III) bound to humic acid in one third of our samples representing up to 64% of the total dissolved Mn. These humic complexes were mostly detected in the hydrothermal vent plume and at the redox boundaries of the oxygen minimum zone in the water column. In the hydrothermal plume, the Mn(III)-humic acid stabilized the manganese in solution up to a ~10,000-fold dilution of the venting water. In the upper water column, Mn(III)-humic acid was only detected after a squall and rain event, which indicates that it is a transient species, persistent over days to weeks. This temporal variability highlights the importance of non-steady-state processes in the open ocean, which may help to explain previous observations of a dissolved Mn maximum within oceanic oxygen minimum zones.

Introduction

The vertical distribution of total dissolved manganese in the East Pacific margin is usually depicted with three concentration maxima: at the surface, in the oxygen minimum zone and, where present, in hydrothermal vent plumes (*e.g.* Klinkhammer and Bender 1980; Martin et al. 1985; Resing et al. 2015). For the first maximum at the surface, the principal source of dissolved Mn is atmospheric dust deposition dissolved by photoreduction (*e.g.* Guieu et al., 1994; Mendez et al., 2010; Sunda et al., 1983) and, of lower magnitude, by efflux of dissolved Mn(II) from coastal sediment (*e.g.* McManus et al., 2012). Sunda and Huntsman (1988) showed that high surface dissolved Mn concentration is also maintained due to photoinhibition of biological Mn oxide formation. In the surface ocean maximum, the removal of dissolved Mn occurs primarily via biological uptake, adsorption onto particles and abiotic and biotic oxidation to solid Mn(III/IV) oxides (Sunda and Huntsman 1990).

In the oxygen minimum zone, several Mn sources have been considered for the second dissolved Mn maximum, fueling a debate between three models explaining the dissolved Mn maximum (Klinkhammer and Bender 1980): model A, the dissolution of Mn oxides in the oxygen minimum zone due to the *in situ* low dissolved oxygen/low pH (Klinkhammer and Bender 1980; Lam et al. 2018); model B, the offshore transport of sediment porewater efflux favored by the slow oxidation kinetics of Mn(II) in the oxygen minimum zone (*e.g.* Martin and Knauer 1984; Lewis and Luther III 2000; Cutter et al. 2018); and model C, the release of dissolved Mn by mineralization of organic matter (Johnson et al. 1996; Vedamati et al. 2015; Sanial et al. 2017). There are two common assumptions regarding Mn redox chemistry within these three models. First, they assume that the total dissolved Mn pool is comprised of only Mn(II), whereas recently, much work has reported on

the environmental importance of dissolved Mn(III) bound to organic ligands (*e.g.* Trouwborst et al. 2006; Madison et al. 2011; Jones et al. 2020) and laboratory results have shown that certain organic and inorganic ligands prevent dissolved Mn(III) disproportionation for weeks (*e.g.* Kostka et al., 1995). However, these prior field studies have only examined estuarine water columns and sediment porewaters, with dissolved Mn concentration exceeding 20 nM. More recent investigations on the continental shelf of the Northwest Atlantic ocean (Oldham et al. 2020) and into the open ocean waters of the Northwest Atlantic Ocean (Jones et al. 2020) report important contributions of Mn(III) to the total dissolved Mn pool, though decreasing offshore. Jones et al (2020) report increased contributions of Mn(III) in the oxygen minimum zone waters that have a O_2 saturation state of 50%. The first goal of the present study is thus to determine whether Mn(III) is an important component of the total dissolved Mn pool in the open ocean system of the Pacific.

The second assumption of the above models is that they assume the system is at steady state. Sampling during cruises doing transects with short stops on each station favors the interpretation of changes due to vertical and lateral heterogeneity rather than temporal variation. However, storms and/or eddies are known to change, sometimes drastically, the water column properties (*e.g.* Babin et al., 2004). This could be especially important for metastable species, such as dissolved Mn(III), since its stability depends on the complex(es) it forms. Thus, our second goal is to address this potential for temporal variability in the stabilization of dissolved Mn(III); to this aim, we sampled the water column over the course of three weeks at the same station above the East Pacific Rise hydrothermal vent system, 900 km south of Mexico and 2000 km west of Costa Rica.

In the deep ocean, the third dissolved Mn maximum is a well-known feature of active hydrothermal sources which release dissolved Mn suspected to be Mn(II) (*e.g.* Klinkhammer et al., 1977). This dissolved Mn can be transported vertically several hundred meters above the vent

source and can also be transported laterally hundreds to thousands of kilometers (Fitzsimmons et al. 2014). Possible removal processes from vent sources include bacterial dissolved Mn(II) oxidation in the vent water (Ehrlich, 1983; Dick et al., 2006; Mandernack and Tebo, 1993) and in the plume (Cowen et al. 1986), as well as abiotic dissolved Mn(II) oxidation and/or adsorption onto particles (Mandernack and Tebo 1993). Therefore, the third goal of our work is to characterize the importance of organic ligands capable of stabilizing dissolved Mn(III) in the East Pacific Rise (EPR) hydrothermal plume. The vent work reported here builds on the chemistry that our group (Shaw et al, 2021) found in the dynamic mixing zone from the vent orifice to about 3 meters above the vent, which is the origin of the vent plume. In Shaw et al (2021), we showed that dissolved Mn(III) was produced due to the formation of reactive oxygen species as the thermodynamics of Mn(II) oxidation by O_2 is not favorable (Luther, 2010). Here, we show that dissolved Mn(III) formed in the dynamic mixing zone is transported in the resulting plume into the water column.

Overall, this study tries to answer A) Is Mn(III)-ligand an important component of the total dissolved Mn pool in the open ocean ? B) How does temporal variability affect the distribution of Mn(III)-ligand ? and C) Is Mn stabilized as a complex by organic ligand in the vent plume?

Materials and methods

Seawater sampling

Four vertical water column profiles of chemical and physical properties were performed at 9º 50′ N East Pacific Rise (104º 17′ W) on April 3, 6, 13 and 15 of 2017 aboard the R/V *Atlantis*. A squall, with average wind speed of 40 km h^{-1} associated with 10 mm of rain, occurred on April 11th and 12th, 2017. During each cast, 12 depths were sampled in duplicate using a 24-Niskin bottle rosette equipped with a Seabird 911 CTD (Conductivity, Temperature, Depth) profiler as well as oxygen (SBE43), fluorescence (Wetlabs FLNTURTD) and beam transmission (Wetlabs C-Star transmissometer) sensors. The Oxygen sensor has a reported detection limit of 3 μM with high stability (shift < 1 μM/month). As our profiles occurred over a 12-day period and the O_2 concentration difference before and after the squalls was > 2 μM, we regard comparisons at low O_2 concentrations as reliable because of the sensor's high stability. In addition to these sensors, a transponder was put on the CTD rosette to communicate with a deep ocean transponder placed via the HOV *Alvin* so that the rising plume could be better detected, and samples could be obtained closer to the source hydrothermal vents. The transponder allowed us to sample in or nearer the vent plume than could be done in other work (e.g., Fitzsimmons et al 2017; Lam et al, 2018).

The sampling was focused above, within and below the oxygen minimum zone and, in particular, along the oxygen decrease from the surface to the top of the oxygen minimum zone, as determined by the *in situ* dissolved oxygen profile. Water samples were obtained thanks to 10-liter external spring trace metal Niskin bottles by General Oceanics, acid cleaned on deck prior to deployment. Blanks showed negligible Mn contamination. Two liters aliquots were collected using acid-washed tubing into acid-washed LDPE bottles after triplicate rinsing, and minimizing atmospheric oxygen

contamination by overflowing bottles. Samples were filtered by vacuum pump within 1 hour of collection through 47 mm diameter 0.2 µm acid cleaned membrane filters (polycarbonate from Whatman®, in a N_2-filled glove bag for oxygen minimum zone samples) using acid-cleaned polycarbonate filtration units (Savillex). Filtered samples were not acidified but frozen and preserved at -20^{o}C until analysis.

Dissolved Mn speciation measurements

Dissolved Mn speciation was measured by UV-vis adsorption at 468 nm of a Mn-porphyrin complex formed after a Cd(II)-porphyrin reagent addition to the sample (Ishii et al. 1982). Details of the method are described in Thibault de Chanvalon and Luther 2019. The final concentrations of the Cd(II)-porphyrin reagent components after mixing with the sample are: sodium tetraborate (500 µM), imidazole (18 mM), T(4-CP)P porphyrin (240 nM) and $CdCl_2$ (24 µM). The UV-vis adsorption was measured in a 500-cm long wave capillary cell (World Precision Instrument) which gives a detection limit of 0.3 nM (3x times the blank's standard deviation). Three discrete aliquots of a sample are measured in triplicate (Table 1). These aliquots divide the total dissolved Mn pool into three conceptual fractions in Table 1 (dissolved Mn(II); dissolved Mn(II) and Mn(III)-humic acid; total dissolved Mn), which are distinguishable by the chemical properties of each fraction.

The “heated only” aliquot corresponds to the measurement after 60 minutes of reacting in a 90 ^{o}C water bath and corresponds to the complexation of Mn(II) and any weak and fast reacting Mn(III) complexes. For simplicity, we refer to this fraction as Mn(II) even if it includes some Mn(III)-ligand$_{weak}$ (log K_{cond} < 11.6) described previously (Madison et al. 2011).

The “HA removed” aliquot is acidified (pH<2) and filtered prior to the reagent addition and similar heating and causes removal of the associated Mn (Oldham et al., 2017a,b). Since Mn(II)

binds very weakly to organic matter (Irving and Williams 1948; Madison et al. 2011), we assume that the Mn precipitating with humic materials is Mn(III) (Mn(III)-humic acid). The Mn remaining in solution after acid precipitation is Mn(II). Thus, the difference between dissolved Mn in the heated fraction and the Mn(II) in the solution after acid precipitation of humic acids provides the concentration of Mn(III)-humic acid. We note that humic material in waters near vents can come from several sources including the vents, chemosynthetic organisms surrounding vents and bottom waters; functional groups include hydroxylated aromatic and nonaromatic compounds that can bind metals (Luther 2021).

Finally, the "NH_2OH reduced" aliquot is treated with a strong reducing agent, NH_2OH (final concentration of 100 nM), to reduce all Mn(III)-ligand compounds to Mn(II) before addition of the Cd(II)-porphyrin reagent and heating. In this latter case, both Mn(II), Mn(III)-humic acid and any manganese bound to a strong ligand (Mn(III)-$ligand_{strong}$) are complexed by the Cd(II)-porphyrin reagent. This measurement gives the total dissolved Mn concentration.

In Thibault de Chanvalon and Luther (2019), we reported that the method agrees with other methods on known standards. We measured total manganese [after the heating treatment (Mn(II)+ Mn(III)-$ligand_{weak}$ + Mn(III)-humic acid)] using the Canadian NASS-6 standard material at 10.1 ± 0.7 nM (n=12, consensus NASS value of 9.65 ± 0.92 nM) and in the Geotraces SAFe-S material at 0.82 ± 0.17 nM (n=9, consensus SAFe-S value of 0.825 ± 0.08 nM).

Table 1: correspondence between analyses and expected speciation measured

Dissolved Mn Analyses	**Expected speciation measured**
HA removed	Mn(II)
Heated only	Mn(II) + Mn(III)-humic acid

NH_2OH reduced	Mn(II)	+ Mn(III)-humic acid	+ Mn(III)-$ligand_{strong}$

159

Results

CTD data and identification of water masses

The salinity and temperature profiles of the water column (Figure 1) permit identification of 4 main water masses.

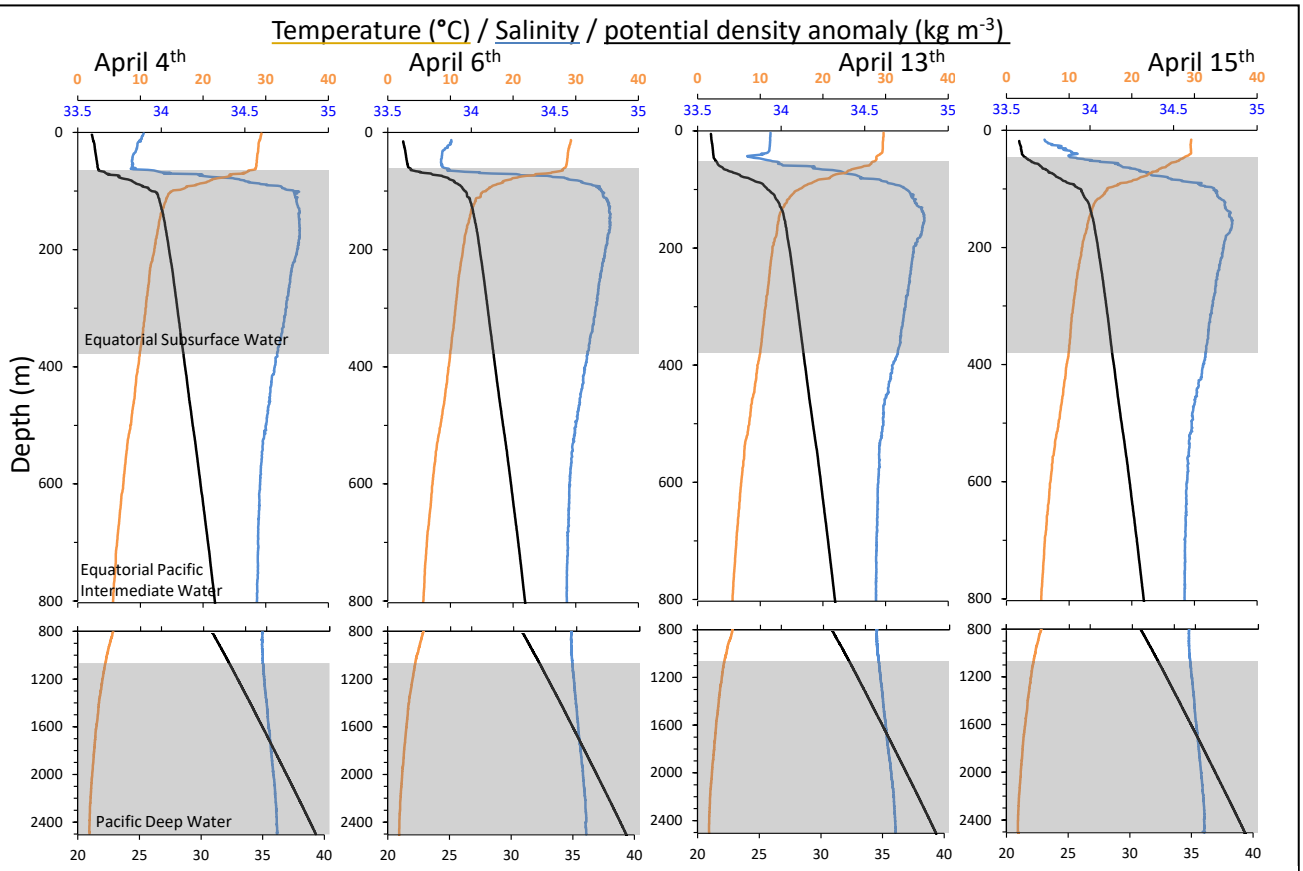

Figure 1: CTD profiles with shaded areas identifying the main water masses. Temperature in orange, salinity in blue and potential density anomaly in black.

(1) The surface layer (21 < σ_θ (potential density anomaly) < 21.6) with low salinity, high temperature and high oxygen concentration, extended from the surface down to 65 ± 5 m depth. This depth also corresponded to the fluorescence maximum and to the beam transmission minimum (Figure 2). The squall (11th and 12th April) impacted the water column properties and raised the start of the dissolved oxygen gradient from 68 to 55 m depth (Figure 3A). However, these depths corresponded to an identical potential density (σ_θ = 21.6), which

indicates that the elevation of the oxygen gradient is produced by an increase of mixing between the surface layer and the layer beneath.

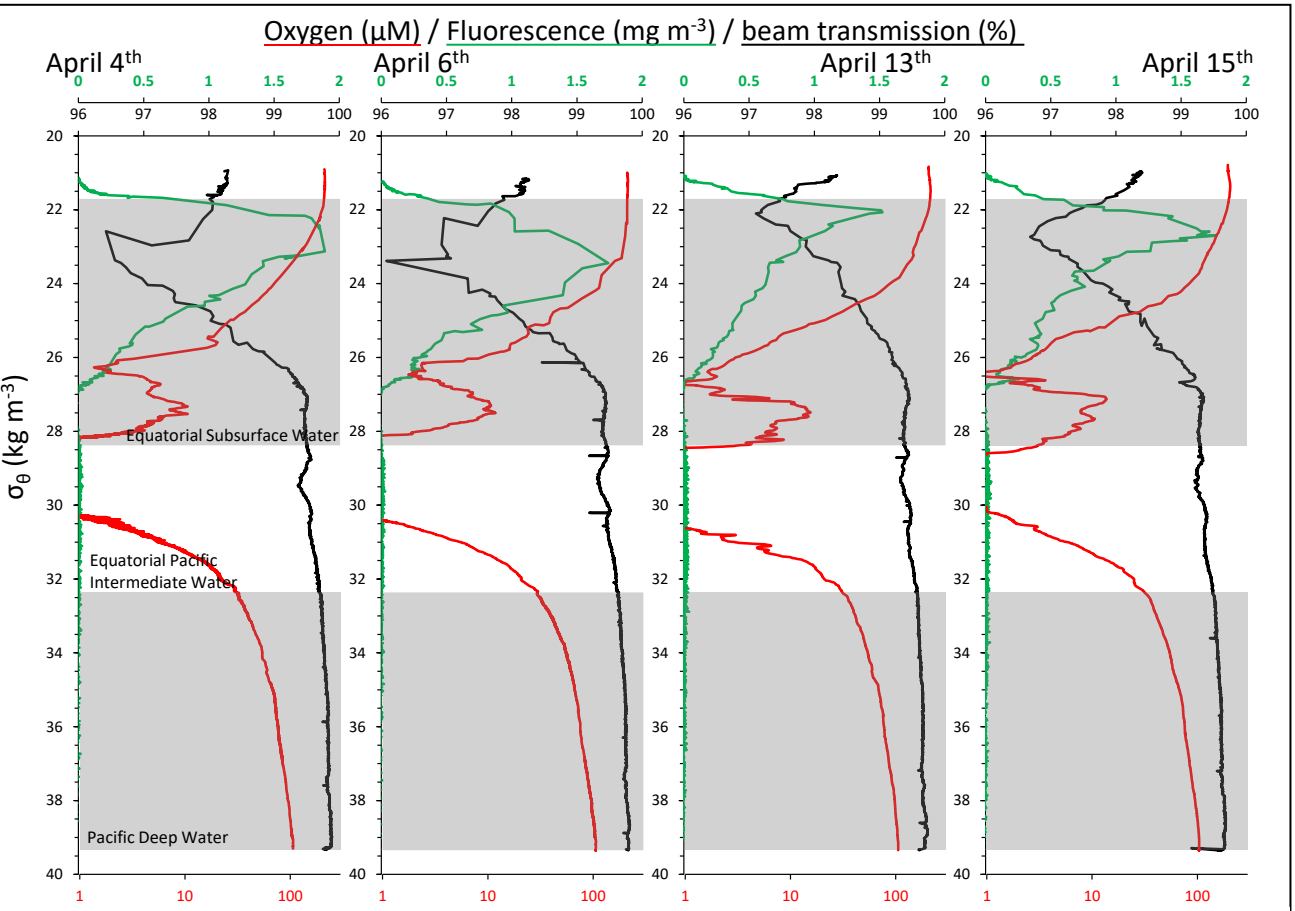

Figure 2: CTD profiles with shaded areas identifying the main water masses. Oxygen (in red) concentrations have a logarithmic scale. Beam transmission is in black, fluorescence in green.

(2) The Equatorial Subsurface Water (Peters et al., 2017) between ~ 70 m and ~ 400 m depth ($21.6 < \sigma_\theta < 28.4$) is characterized by high salinity and an oxygen concentration that drops sharply, reaches a first minimum at $\sigma_\theta = 26.6$, then varies between 1 µM and 15 µM (Figure 2). In this layer, the impact of the squall is visible on the oxygen minimum of the Equatorial Subsurface Water that decreases from 3 µM to < 1 µM at 120 m depth (Figure 3B). Moreover, at the lower Equatorial Subsurface Water limit (~ 400m depth), the weakly oxygenated water (between 1 µM and 15 µM) expands downward after the squall (Figure 3C) suggesting a possible increase of water mixing down to this depth.

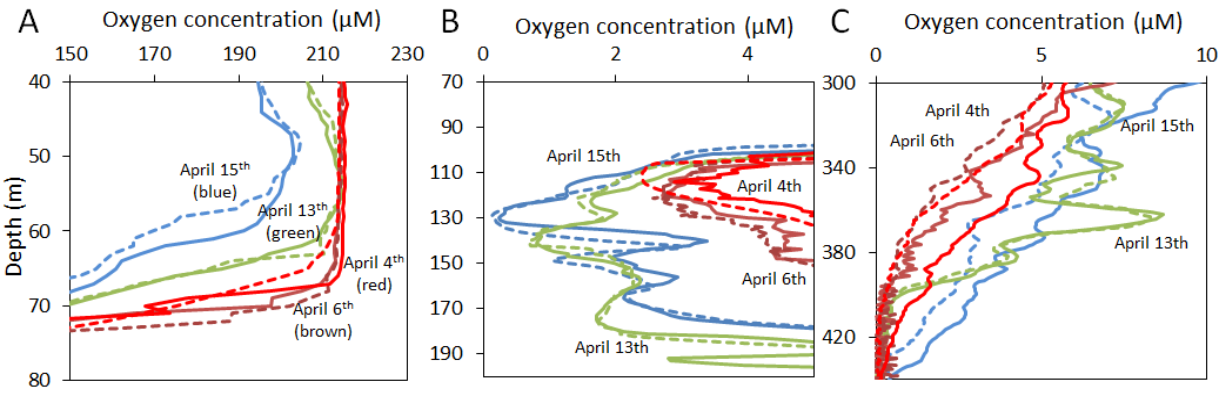

Figure 3: Details of oxygen profiles from the CTD: A - at the boundary between surface layer and Equatorial Subsurface Water; B –at the top of the Equatorial Subsurface Water and C – at the boundary between Equatorial Subsurface Water/Equatorial Pacific Intermediate Water. Solid lines correspond to downward measurements; dotted lines correspond to upward measurement.

(3) The Equatorial Pacific Intermediate Water (Figure 1), between ~ 400 m and ~ 1100 m depth ($28.4 < \sigma_\theta < 32.4$), is characterized by an oxygen depletion with concentration mostly below the sensor's detection limit of 3 µM. Two weak beam transmission maxima are constant over time at $\sigma_\theta = 29.5$ and $\sigma_\theta = 30.6$ (Figure 2).

Below the Equatorial Pacific Intermediate Water is the (4) Pacific Deep Water, with density above $\sigma_\theta = 32.4$. This zone is characterized by low temperature and high concentrations of oxygen. Close to the bottom (at 2500 m depth), a decrease of beam transmission was observed on the 4th, 13th and 15th April because the CTD was in the plume produced by the active vents of the East Pacific Rise.

Manganese speciation

The manganese concentrations obtained with the methods "heated only" and "NH_2OH reduced" show similar results (Table 2). According to the operational definitions from Table 1, this indicates that there is no Mn(III)-ligand$_{strong}$ present in our samples. Because of these similarities, we describe total dissolved Mn using the results from the "heated only" method. In contrast, the results from

194 the acidified, "HA removed" method showed lower dissolved Mn values than the non-acidified
195 method in 31% of the samples, indicating Mn removal during the acidification step. Mn is likely
196 to be removed during the acidification if it is bound to humic material, which precipitates at pH<2,
197 and if it is not dissociated from its ligand (Oldham et al., 2017a,b). Therefore, the Mn(III)-humic
198 acid is calculated by difference between the "heated only" and "HA removed" methods (Table 1).

199 Table 2: Slope (a) and correlation coefficient between the concentrations
200 measured with the methods "heated only" and "NH2OH reduced"

Date	"heated only" versus "NH_2OH reduced"
April 4th	a = 1.01 r^2 = 0.82
April 6th	a = 1.00 r^2 = 0.72
April 13th	no data
April 15th	no data

201 The concentrations of total dissolved Mn before the squall (4th and 6th April, Figure 4 and
202 Supporting Information Table S1) correspond to previous manganese profiles from this region
203 (Klinkhammer and Bender 1980; Murray et al. 1983) with surface concentrations between 2.6 and
204 2.9 nM. A second maximum occurs at the oxycline, with values of 5.3 and 3.7 nM for April 4th and
205 6th, followed by a decrease in the Equatorial Subsurface Water (total dissolved Mn = 2.6 and 2.4
206 nM). A third maximum is visible in the center of the oxygen minimum zone (4.4 and 3.7 nM for
207 April 4th and 6th) and lower concentrations (2.3 nM) are observed in the Pacific Deep Water at 1500
208 m depth. No Mn(III)-humic acid complexes were detected in the water column before the squall
209 with the exception of above the hydrothermal vent.

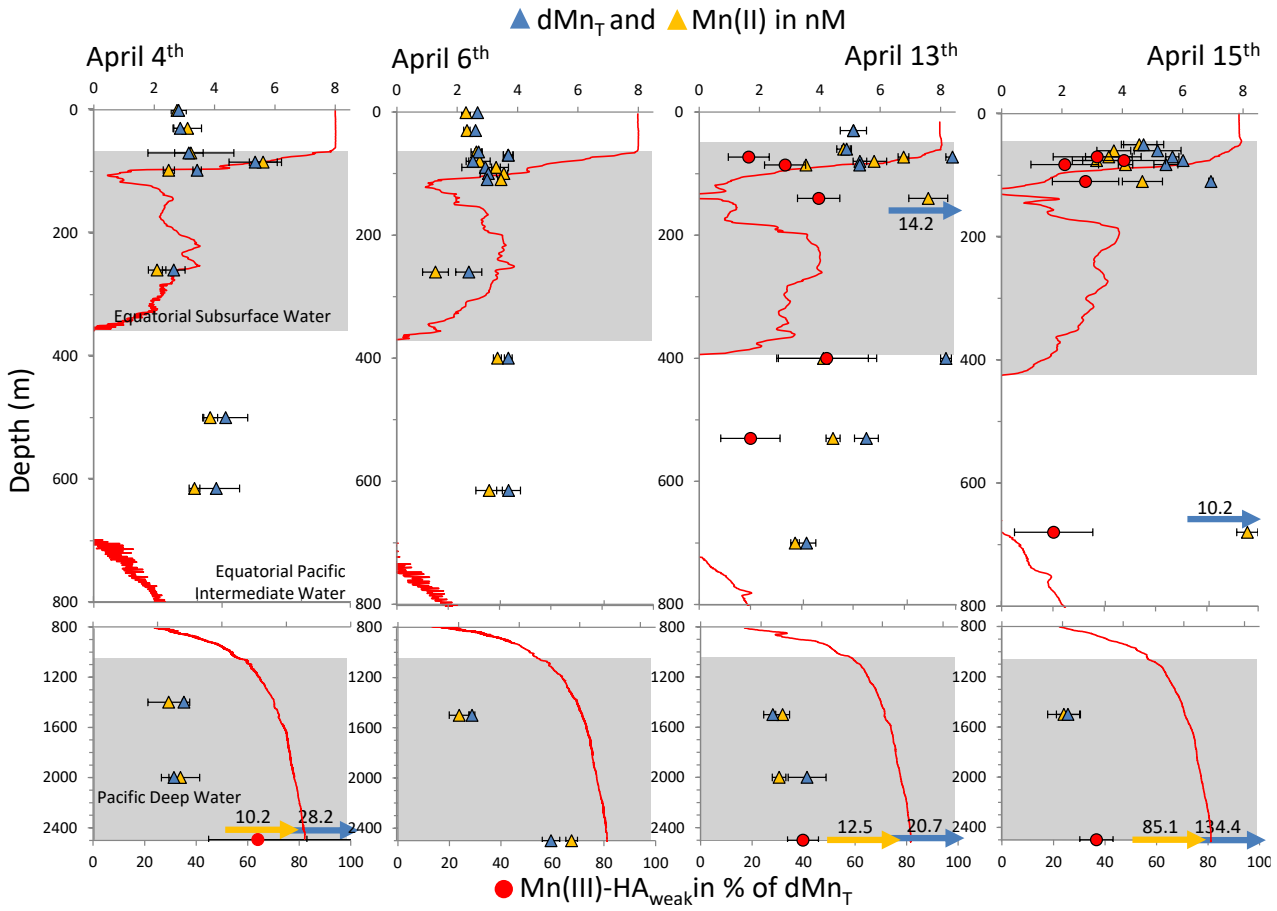

Figure 4: Manganese speciation above 9° 50′ N East Pacific Rise with shaded areas identifying the main water masses. Oxygen profile is superimposed for reminder. dMn_T (total dissolved Mn) and Mn(II) are the upper x-axis whereas Mn(III)-humic acid in % of dMn_T is the lower x-axis.

After the squall, the total dissolved Mn concentrations increased at the surface (Figure 4, April 13th and 15th) up to 5 nM (at 30 m depth), likely due to the dissolution of dust deposition associated with the rain event, but no form of dissolved Mn(III) was identified. Although we have no data from aerosol samples, Marsay et al. (2022) and Buck et al. (2019) show that Mn from crustal sources is present in dust samples from the Eastern and Central Pacific, respectively, indicating that Mn was deposited to our surface waters after the rain event.

At the oxycline, total dissolved Mn concentration increased after the squall up to 8.4 nM and was composed of, on average, 33% Mn(III)-humic acid (Table 3). At 140 m depth, in the Equatorial

Subsurface Water, a particularly high total dissolved Mn concentrations (14.2 nM) associated with the detection of Mn(III)-humic acid was also observed and coincided with an oxygen decrease during the squall (from 3 µM to < 1 µM, Figure 3B). Finally, at the boundaries of the oxygen minimum zone (400 and 680 m depth), an increase of total dissolved Mn (up to 8.1 nM at 400m depth and 10.2 nM at 680 m depth) associated with Mn(III)-humic acid is observed after the squall.

Table 3: Beam transmission and temperature signature of bottom water (depth = 2504 ± 6 m) compared to the manganese speciation. The dilution factor is calculated based on the bottom water change of Temperature compared to the measured temperature of the closest venting water.

Date	Location	Closest vent	Bottom change of beam transmission	Bottom change of Temperature (°C)	Temperature of venting water (°C)	total dissolved Mn (nM)	Mn(III)-humic acid (% total dissolved Mn)	Dilution factor
April 4th	9°50.97N 104°17.62W	BioVent	-0.13 %	+0.05	310	28.2	64	5740
April 6th	9°47.25N 104°16.97W	V Vent	0.0 %	0.0	ND	5	0	>20000
April 13th	9°50.31N 104°17.48W	Bio 9 Vent	-0.08 %	+0.04	370	20.7	40	9250
April 15th	9°50.15N 104°17.46W	P Vent	-0.7 %	+0.13	360	134.4	37	2950

Above the hydrothermal vents (~10 m), the beam transmission shows attenuation on April 4th, 13th and 15th due to the particles carried by the vent plume (Figure 2) while the temperature increases. The bottom changes of both temperature and beam transmission were obtained from a close look at the data from the ten deepest meters obtained during the CTD casts (Supporting Information Fig. S1). Table 3 shows the strong relationship between the bottom changes of beam transmission and temperature increases ($r^2 > 0.9$) along with an increase in dissolved Mn, indicating that vent fluid emission is the major source of dissolved Mn in this system. In particular, Figure 5 shows that Mn(III)-humic acid increase linearly with temperature anomalies with a slope of 320 ± 100 nM $°C^{-1}$ and account for 37 - 64% of total dissolved Mn while dissolved Mn(II) presents an

236 important loss between temperature anomalies of 0.13 ºC and 0.05 ºC. In contrast, on the 6th of

237 April, we did not detect a plume (no beam transmission nor temperature anomaly) and there were

238 lower total dissolved Mn concentrations (5 nM) and no detectable Mn(III)-humic acid.

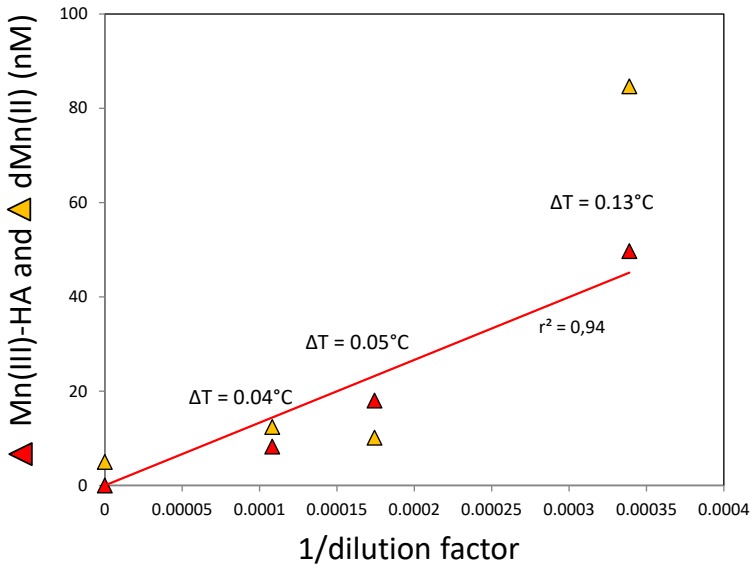

Figure 5: Manganese speciation in the hydrothermal plume (depth = 2504 ± 6 m, data from Table 3). dMn(II) is dissolved Mn(II) and ΔT is temperature anomalies.

239

240

Discussion

On April 11th and 12th, a squall with average wind speed of 40 km h^{-1} and a rainfall of 10 mm occurs simultaneously to significant water mixing. At redox gradient depths, after the squall, an important increase of total dissolved Mn was observed, in association with dissolved Mn(III). The three first parts of the discussion propose explanations for these changes comparing the situation before to the situation after the squall. The last part of the discussion focuses on the role of hydrothermal vents whose plume was always associated with important Mn (III) contribution.

Mn speciation before the squall (surface and Oxygen minimum zone)

For the April 4th and 6th samplings, dissolved Mn speciation indicates that only dissolved Mn(II) is detected except above the hydrothermal vent on April 4 (Table S1). April 4th and 6th dissolved Mn profiles (Figure 4) present the typical features across the oxygen minimum zone including a sharp peak of total dissolved Mn concentration at the oxycline up to 5.3 nM, as recently observed in other oxygen minimum zones (Vedamati et al. 2015; Sanial et al. 2017) and a broader increase of total dissolved Mn (up to 4.4 nM) in the core of the oxygen minimum zone reported in this region since the 1980s (Klinkhammer and Bender 1980; Martin and Knauer 1984). Three models can independently explain these observations alone or in combination: the dissolution of Mn oxides settling from the mixed layer (model A, Klinkhammer and Bender, 1980; Lam et al., 2017); the offshore transport of sedimentary efflux in a context of slow dissolved Mn removal by reoxidation due to the oxygen minimum zone (model B, Martin and Knauer, 1984; Lewis and Luther III, 2000; Cutter et al., 2018) or the *in situ* mineralization of organic matter associated also with slow oxidation (model C, Johnson et al., 1996; Vedamati et al., 2015; Sanial et al., 2017). The absence of measurable dissolved Mn(III) on April 4th and 6th samples bring new information of the ongoing processes. Indeed, previous studies over a natural redox gradient in the Black Sea (Trouwborst et

al. 2006; Yakushev et al. 2009), estuaries (Oldham et al. 2017b; a; Jones et al. 2019) and porewaters (Madison et al. 2013) demonstrate the ubiquity of dissolved Mn(III) where intense redox reactions occur. The production of dissolved Mn(III) during Mn oxide reduction is further supported by laboratory experiments (Stone 1987; Perez-Benito 2002) including electrochemical (Ruppel et al. 2001), ligand driven (Duckworth and Sposito 2007) and bacterial reduction (Lin et al. 2012). Finally, thermodynamic considerations also highlight the efficiency of two one-electron transfer steps versus a single two-electron step (Luther 2005; Luther et al. 2018) which also supports the formation of intermediate Mn(III) during redox reactions. Thus, the absence of dissolved Mn(III) before the squall (on April 4^{th} and 6^{th} samples; Figure 4) implicates a weak intensity of redox reactions such as Mn(IV) oxide reduction to dissolved Mn(II) which favors models B or C over model A.

Mn speciation after the squall (surface and Oxygen minimum zone)

After the squall (on April 13^{th} and 15^{th}), changes of temperature, salinity and oxygen gradient (Figure 1, Figure 2 and Figure 3A) indicate important mixing between the oxygenated mixed layer and the low oxygenated Equatorial Subsurface Water that would stimulate redox reactions. The notable increase of total dissolved Mn (Figure 4, April 13^{th} and 15^{th}) indicates new atmospheric input of manganese in the water column while the appearance of Mn(III)-humic acid suggests significant redox recycling. A significant wet deposition of Mn during the squall followed by the reductive dissolution of Mn(III/IV) oxides can explain these observations (model A). The models B and C are not likely since there is no indication of an increase of transport rate of the sedimentary efflux (model B) nor an increase of organic matter degradation (model C). Contrastingly, oxide reduction is supported by the presence of sufficient reductants in the top of the east Pacific oxygen minimum zone (*e.g.* Vedamati et al., 2015; Cutter et al., 2018) such as Fe^{2+} (Hartman et al. 1984;

Van Cappellen and Wang 1996), NH_3 (Luther et al. 1997), dissolved organic matter (Stone and Morgan 1984) or NO_2^- (Bartlett 1981; Lewis and Luther III 2000). Additionally, the reducing conditions in the upper oxygen minimum zone are reinforced after the mixing event with an oxygen concentration that decreases (Figure 3B). However, the wet dust input is probably limited to the top of the oxygen minimum zone while, in our dataset, some increase of total dissolved Mn and Mn(III)-humic acid is also found at 400 and at 700 m depths, with concentrations reaching up to 8.2 nM and 10.2 nM respectively. These latter data suggest the occurrence of another source of manganese oxides that are mixed and reduced within the oxygen minimum zone during the squall. Contamination is unlikely since these two data points were processed simultaneously with other samples, and, in addition, samples from two different Niskin bottles from each depth show consistency. While surprising, these high values could be explained by the reduction of subsurface Mn oxides transported by horizontal eddies, which are very common in this region (Kessler 2006; Cole et al. 2015).

Lifetime of Mn(III)-humic acid in the oxygen minimum zone

The lifetime of Mn(III)-humic acid depends on the properties of the humic ligands that stabilize Mn(III). At our site, the lifetime of Mn(III)-humic acid is longer than 3 days (the time between the squall and our measurements) and is shorter than the delay since the last squall, probably about one month, as Mn(III)-humic acid was not observed before the squall. This lifetime may limit the role of Mn(III)-humic acid ligands in stabilizing dissolved Mn during long-term transport. Additionally, the Mn(III)-humic acid is recovered in both the "NH_2OH reduced" and the "heated only" aliquots, which indicates a quite rapid dissociation constant ($k_d > 2.8 \times 10^{-4}\ s^{-1}$; Luther et al. 2015). If we assume a formation constant (k_f) equal to $10^9\ M^{-1}\ s^{-1}$, as in Luther et al. (2015), it corresponds to a stability constant $K_{COND}=k_f/k_d$ inferior to $10^{12.6}$. This weak complexation of the HA ligands

corresponds to the findings of Oldham et al. (2017b) in estuarine waters but contrasts with the St. Lawrence Estuary waters, where Oldham et al. (2017c) showed that Mn(III)-humic acid was included in the "NH_2OH reduced" aliquots but not in the "heated only" aliquots. To sum up, the occurrence of a metastable redox state of dissolved Mn demonstrates the non-equilibrium state of Mn in the water column in proximity of important redox gradients, and highlights the importance of short-term temporal effects that impact Mn cycling after a storm event. Taking into account this variability, we suggest that offshore transport of sediment efflux or organic matter remineralization (model B and C) control the Mn concentration at the steady state, but that the redox dissolution becomes more important after mixing events (model A). These features are usually not described because most samples come from cruises that do not stay at the same location for more than one sampling.

Impact of hydrothermal vents on dissolved Mn distribution

The increase of dissolved Mn at the bottom of our water column profile, due to hydrothermal venting, is revealed by the increase of dissolved Mn concentration with temperature anomalies and increased particles as determined by transmissometer (Table 3). The temperature anomalies observed at 0.04, 0.05 and 0.13°C correspond to a vent water diluted 3,000 to 10,000-fold (Table 3). Figure 5 shows that Mn(III)-humic acid behaves conservatively with a slope of 320 ± 100 nM $°C^{-1}$, indicating an absence of reaction in the plume between dilution 3,000 to dilution 10,000. Additionally, an extrapolation up to 28 °C gives a concentration of Mn(III)-humic acid of 10 ± 3 µM, which corresponds to the value measured independently for Mn(III) bound to a strong ligand, from a HOV *Alvin* dive sampling (Shaw et al. 2021) and suggests a continuous Mn(III) stabilization effect of ligands between dilution 10 and dilution 10,000. Thus, a significant quantity of dissolved Mn(III) is produced in proximity of the vent before the plume temperature decreases down to 28

333 °C (dilution 10), probably in few minutes. This formation can be explained by rapid dissolved
334 Mn(II) oxidation in the presence of important humic like material produced by local bacterial and
335 macrofaunal communities (Lang et al. 2006; Longnecker et al. 2018). These two groups showed
336 that there is higher dissolved organic carbon of 5 µM to 14 µM in waters surrounding vents
337 compared to the ambient deep seawater.

338 Conditions in the venting waters are acidic and O_2 depleted (not detected, below 1 µM), which
339 are conditions that prevent dissolved Mn(II) oxidation (Stumm and Morgan 1996; Morgan 2005;
340 Luther 2010). However, the mixing of cold oxygenated water with hot reducing waters rich in Fe^{2+}
341 and H_2S produce a dynamic reaction zone that leads to reactive oxygen species formation as the
342 direct reaction of Fe^{2+} with O_2 is thermodynamically favorable but the reaction of Mn^{2+} is not
343 favorable (Luther, 2010). Shaw et al. (2021) demonstrated an oxidative pathway involving reactive
344 oxygen species as H_2O_2 was detected up to 6.2 µM. In particular, while overall oxidation by O_2 is
345 faster for Fe(II) than for Mn(II) leading to O_2^-, O_2^- reacts faster with Mn(II) to produce H_2O_2 by an
346 order of magnitude (Rush and Bielski 1985; Barnese et al. 2012). Therefore, as for Fe(III) (Bennett
347 et al. 2008) and Cu(II) (Sander et al. 2007), organic ligands stabilize dissolved manganese released
348 by hydrothermal vents, in this case as a metastable Mn(III) complex. Overall, the sequence of
349 reactions is given to form Mn(III) by the following equations (1-3):

350 (1) $Fe^{2+} + O_2 \rightarrow Fe^{3+} + O_2^-$

351 (2) $O_2^- + Mn^{2+} + 2\,H^+ \rightarrow Mn^{3+} + H_2O_2$

352 (3) $Mn^{3+} + \text{ligand} \rightarrow \text{Mn(III)-ligand}$

353 Fe^{3+} can also react with L to form Fe(III)-L as well as with H_2S to reform Fe^{2+}, and acts as a
354 catalyzer of the Mn oxidation (Shaw et al, 2021).

Figure 5 shows dissolved Mn(II) removal in the concentrated plume as expected from previous studies (*e.g.* Lupton et al., 1980; Resing et al., 2015; Fitzsimmons et al., 2017) but this trend is observed only with one point, the less diluted one. Our dataset indicates that no Mn(III)-humic acid is formed in the concentrated plume which suggests the absence of direct Mn(II) oxidation and contrasts with the Mn(III)-humic acid production in the venting water. The removal could indeed be produced by adsorption onto particles or biological uptake.

The April 6 data show no temperature anomalies in agreement with no detection of Mn(III)-humic acid. However, the 5 nM total dissolved Mn we measured is much higher than the oceanic end member, indicating that at dilution above 20,000, the plume contains only dissolved Mn(II) and no Mn(III)-humic acid. Similar diluted plume water from the East Pacific Rise at 15°S showed a dissolved Mn concentration of 15 nM (Resing et al. 2015) and was about one month old according to radium isotopes (Kipp et al. 2018). Assuming a similar order of magnitude between East Pacific Rise at 15°S and at 9°50'N, we can roughly estimate that the April 6th data point with dissolved Mn(II) = 5 nM is about one month old. Thus, the Mn(III) stabilization by the humic ligand is transient, the Mn(III)-humic acid being removed after about a month in diluted plume as it is in the ocean water column (see §5.2.3).

To sum up, dissolved Mn(III) is produced in the venting plume due to partial dissolved Mn(II) oxidation when reactive oxygen species are produced; the dissolved Mn(III) is simultaneously stabilized by humic like materials. While transported away and progressively diluted (from 10 to 10,000 fold) part of the dissolved Mn(II) pool seems to be removed, probably by adsorption onto particles, while dissolved Mn(III) stays in solution. Then, farther away, once the plume dilution exceeds 10,000, the particles are less concentrated and dissolved Mn(II) removal becomes ineffective (e.g. Mottl et al., 1995), whereas metastable Mn(III)-humic acid has reacted to form

stable dissolved Mn(II) or particulate Mn(IV) and is no longer detected. A key to this study was the use of a transponder system on the CTD rosette and on the basalt bottom to sample closer to vent sources so that the concentrated rising plume could be better sampled.

Conclusion

We find significant concentrations of Mn(III) bound to humic acid-type ligands in the Pacific Margin, based on a decrease of the absorbance signal of the Mn-porphyrin complex after acidification and filtration. One third of our samples shows Mn(III)-humic acid occurrence, in particular in the oxic/anoxic transitions characterized by intense mixing, that happen in two oceanic environments, near the vent and in the oxygen minimum zone after the squall. In Shaw et al (2021), we showed that dissolved Mn(III) was produced in the venting water due to the formation of reactive oxygen species. Here, we show that Mn(III)-humic acid is conservative and stable in the concentrated plume while Mn(II) is removed, probably by adsorption. However, in the diluted plume all the Mn(III)-humic acid reacts with the ambient oceanic species and is not measurable. In the steady state water column, no Mn(III)-humic acid was observed, even across the oxygen minimum zone. However, a squall was enough to increase water mixing and stimulate redox reactions, which result in Mn(III)-humic acid formation. These results are in line with the hypothesis that wet Mn oxides deposition followed by reductive dissolution are an important dissolved Mn source for the oceanic Mn cycle. Such events would modify on a short term, less than a month, the biogeochemistry of the top oceanic layer that is not easily sampled by traditional cruises that spend a day per station.

Acknowledgements

This work was funded by grants from the Chemical Oceanography program (OCE-1558738 to GWL; OCE-1558692 to BMT) and the Marine Geology and Geophysics program (OCE-1558712 to GWL) of the National Science Foundation. Thanks to the crew of the R/V *Atlantis* who made sampling for this research possible. The authors declare no conflict of interests.

Bibliography

Babin, S. M., Carton J. A., Dickey T. D., and Wiggert J. D. 2004. Satellite evidence of hurricane-induced phytoplankton blooms in an oceanic desert. J. Geophys. Res. Oceans **109**. doi:10.1029/2003JC001938

Barnese, K., E. B. Gralla, J. S. Valentine, and D. E. Cabelli. 2012. Biologically relevant mechanism for catalytic superoxide removal by simple manganese compounds. Proc. Natl. Acad. Sci. **109**: 6892–6897. doi:10.1073/pnas.1203051109

Bartlett, R. J. 1981. Nonmicrobial Nitrite-to-Nitrate Transformation in Soils 1. Soil Sci. Soc. Am. J. **45**: 1054–1058. doi:10.2136/sssaj1981.03615995004500060009x

Bennett, S. A., E. P. Achterberg, D. P. Connelly, P. J. Statham, G. R. Fones, and C. R. German. 2008. The distribution and stabilisation of dissolved Fe in deep-sea hydrothermal plumes. Earth Planet. Sci. Lett. **270**: 157–167. doi:10.1016/j.epsl.2008.01.048

Buck, C. S., A. Aguilar-Islas, C. Marsay, D. Kadko, and W. M. Landing. 2019. Trace element concentrations, elemental ratios, and enrichment factors observed in aerosol samples collected during the US GEOTRACES eastern Pacific Ocean transect (GP16). Chem. Geol. **511**: 212–224. doi:10.1016/j.chemgeo.2019.01.002

Cole, S. T., C. Wortham, E. Kunze, and W. B. Owens. 2015. Eddy stirring and horizontal diffusivity from Argo float observations: Geographic and depth variability: ARGO EDDY STIRRING AND DIFFUSIVITY. Geophys. Res. Lett. **42**: 3989–3997. doi:10.1002/2015GL063827

Cowen, J. P., G. J. Massoth, and E. T. Baker. 1986. Bacterial scavenging of Mn and Fe in a mid- to far-field hydrothermal particle plume. Nature **322**: 169–171. doi:10.1038/322169a0

Cutter, G. A., J. W. Moffett, M. C. Nielsdóttir, and V. Sanial. 2018. Multiple oxidation state trace elements in suboxic waters off Peru: In situ redox processes and advective/diffusive horizontal transport. Mar. Chem. **201**: 77–89. doi:10.1016/j.marchem.2018.01.003

Duckworth, O. W., and G. Sposito. 2007. Siderophore-promoted dissolution of synthetic and biogenic layer-type Mn oxides. Chem. Geol. **242**: 497–508. doi:10.1016/j.chemgeo.2007.05.007

Ehrlich, H. L. 1983. Manganese-Oxidizing Bacteria from a Hydrothermally Active Area on the Galapagos Rift. Ecol. Bull. 357–366.

Fitzsimmons, J. N., E. A. Boyle, and W. J. Jenkins. 2014. Distal transport of dissolved hydrothermal iron in the deep South Pacific Ocean. Proc. Natl. Acad. Sci. **111**: 16654–16661. doi:10.1073/pnas.1418778111

Fitzsimmons, J. N., S. G. John, C. M. Marsay, C. L. Hoffman, S. L. Nicholas, B. M. Toner, C. R. German, and R. M. Sherrell. 2017. Iron persistence in a distal hydrothermal plume supported by dissolved–particulate exchange. Nat. Geosci. **10**: 195–201. doi:10.1038/ngeo2900

Guieu, C., R. Duce, and R. Arimoto. 1994. Dissolved input of manganese to the ocean: Aerosol source. J. Geophys. Res. Atmospheres **99**: 18789–18800. doi:10.1029/94JD01120

Hartman, J. R., B. M. Foxman, and S. R. Cooper. 1984. Higher valent manganese chemistry. Synthetic, structural, and solution studies on [Mn (catecholate) 3] n-(n= 2, 3) complexes. Inorg. Chem. **23**: 1381–1387.

Irving, H., and R. J. P. Williams. 1948. Order of stability of metal complexes. Nature **162**: 746–747.

Ishii, H., H. Koh, and K. Satoh. 1982. Spectrophotometric determination of manganese utilizing metal ion substitution in the cadmium-α, β,-γ, δ-tetrakis (4-carboxyphenyl) porphine complex. Anal. Chim. Acta **136**: 347–352.

Johnson, K. S., K. H. Coale, W. M. Berelson, and R. M. Gordon. 1996. On the formation of the manganese maximum in the oxygen minimum. Geochim. Cosmochim. Acta **60**: 1291–1299.

Jones, M. R., G. W. Luther, and B. M. Tebo. 2020. Distribution and concentration of soluble manganese(II), soluble reactive Mn(III)-L, and particulate MnO2 in the Northwest Atlantic Ocean. Mar. Chem. **226**: 103858. doi:10.1016/j.marchem.2020.103858

Jones, M. R., V. E. Oldham, G. W. Luther, A. Mucci, and B. M. Tebo. 2019. Distribution of desferrioxamine-B-extractable soluble manganese(III) and particulate MnO2 in the St. Lawrence Estuary, Canada. Mar. Chem. **208**: 70–82. doi:10.1016/j.marchem.2018.11.005

Kessler, W. S. 2006. The circulation of the eastern tropical Pacific: A review. Prog. Oceanogr. **69**: 181–217. doi:10.1016/j.pocean.2006.03.009

Kipp, L. E., V. Sanial, P. B. Henderson, P. van Beek, J.-L. Reyss, D. E. Hammond, W. S. Moore, and M. A. Charette. 2018. Radium isotopes as tracers of hydrothermal inputs and neutrally buoyant plume dynamics in the deep ocean. Mar. Chem. **201**: 51–65. doi:10.1016/j.marchem.2017.06.011

Klinkhammer, G., M. Bender, and R. F. Weiss. 1977. Hydrothermal manganese in the Galapagos Rift. Nature **269**: 319–320. doi:10.1038/269319a0

Klinkhammer, G. P., and M. L. Bender. 1980. The distribution of manganese in the Pacific Ocean. Earth Planet. Sci. Lett. **46**: 361–384.

Kostka, J. E., G. W. Luther, and K. H. Nealson. 1995. Chemical and biological reduction of Mn(III)-pyrophosphate complexes: Potential importance of dissolved Mn(III) as an environmental oxidant. Geochim. Cosmochim. Acta **59**: 885–894.

Lam, P. J., J.-M. Lee, M. I. Heller, S. Mehic, Y. Xiang, and N. R. Bates. 2018. Size-fractionated distributions of suspended particle concentration and major phase composition from the U.S. GEOTRACES Eastern Pacific Zonal Transect (GP16). Mar. Chem. **201**: 90–107. doi:10.1016/j.marchem.2017.08.013

Lang, S. Q., D. A. Butterfield, M. D. Lilley, H. Paul Johnson, and J. I. Hedges. 2006. Dissolved organic carbon in ridge-axis and ridge-flank hydrothermal systems. Geochim. Cosmochim. Acta **70**: 3830–3842. doi:10.1016/j.gca.2006.04.031

Lewis, B. L., and G. W. Luther III. 2000. Processes controlling the distribution and cycling of manganese in the oxygen minimum zone of the Arabian Sea. Deep Sea Res. Part II Top. Stud. Oceanogr. **47**: 1541–1561.

Lin, H., N. H. Szeinbaum, T. J. DiChristina, and M. Taillefert. 2012. Microbial Mn(IV) reduction requires an initial one-electron reductive solubilization step. Geochim. Cosmochim. Acta **99**: 179–192. doi:10.1016/j.gca.2012.09.020

Longnecker, K., S. M. Sievert, S. P. Sylva, J. S. Seewald, and E. B. Kujawinski. 2018. Dissolved organic carbon compounds in deep-sea hydrothermal vent fluids from the East Pacific Rise at 9°50′N. Org. Geochem. **125**: 41–49. doi:10.1016/j.orggeochem.2018.08.004

Lupton, J. E., G. P. Klinkhammer, W. R. Normark, R. Haymon, K. C. MacDonald, R. F. Weiss, and H. Craig. 1980. Helium-3 and manganese at the 21°N East Pacific Rise hydrothermal site. Earth Planet. Sci. Lett. **50**: 115–127. doi:10.1016/0012-821X(80)90123-5

Luther, G. W. 2005. Manganese(II) Oxidation and Mn(IV) Reduction in the Environment—Two One-Electron Transfer Steps Versus a Single Two-Electron Step. Geomicrobiol. J. **22**: 195–203. doi:10.1080/01490450590946022

Luther, G. W. 2010. The role of one-and two-electron transfer reactions in forming thermodynamically unstable intermediates as barriers in multi-electron redox reactions. Aquat. Geochem. **16**: 395–420.

Luther, G. W. 2021. Hydrothermal Vents Are a Source of Old Refractory Organic Carbon to the Deep Ocean. Geophys. Res. Lett. **48**: e2021GL094869. doi:10.1029/2021GL094869

Luther, G. W., A. S. Madison, A. Mucci, B. Sundby, and V. E. Oldham. 2015. A kinetic approach to assess the strengths of ligands bound to soluble Mn(III). Mar. Chem. **173**: 93–99. doi:10.1016/j.marchem.2014.09.006

Luther, G. W., B. Sundby, B. L. Lewis, P. J. Brendel, and N. Silverberg. 1997. Interactions of manganese with the nitrogen cycle: alternative pathways to dinitrogen. Geochim. Cosmochim. Acta **61**: 4043–4052.

Luther, G. W., A. Thibault de Chanvalon, V. E. Oldham, E. R. Estes, B. M. Tebo, and A. S. Madison. 2018. Reduction of Manganese Oxides: Thermodynamic, Kinetic and Mechanistic Considerations for One- Versus Two-Electron Transfer Steps. Aquat. Geochem. doi:10.1007/s10498-018-9342-1

Madison, A. S., B. M. Tebo, and G. W. Luther. 2011. Simultaneous determination of soluble manganese(III), manganese(II) and total manganese in natural (pore)waters. Talanta **84**: 374–381. doi:10.1016/j.talanta.2011.01.025

Madison, A. S., B. M. Tebo, A. Mucci, B. Sundby, and G. W. Luther. 2013. Abundant porewater Mn (III) is a major component of the sedimentary redox system. science **341**: 875–878.

514 Mandernack, K. W., and B. M. Tebo. 1993. Manganese scavenging and oxidation at hydrothermal
515 vents and in vents plumes. Geochim. Cosmochim. Acta **57**: 3907–3923.
516 Marsay, C. M., D. Kadko, W. M. Landing, and C. S. Buck. 2022. Bulk Aerosol Trace Element
517 Concentrations and Deposition Fluxes During the U.S. GEOTRACES GP15 Pacific
518 Meridional Transect. Glob. Biogeochem. Cycles **36**: e2021GB007122.
519 doi:10.1029/2021GB007122
520 Martin, J. H., and G. A. Knauer. 1984. VERTEX: manganese transport through oxygen minima.
521 Earth Planet. Sci. Lett. **67**: 35–47.
522 Martin, J. H., G. A. Knauer, and W. W. Broenkow. 1985. VERTEX: the lateral transport of
523 manganese in the northeast Pacific. Deep Sea Res. Part Oceanogr. Res. Pap. **32**: 1405–1427.
524 McManus, J., W. M. Berelson, S. Severmann, K. S. Johnson, D. E. Hammond, M. Roy, and K. H.
525 Coale. 2012. Benthic manganese fluxes along the Oregon–California continental shelf and
526 slope. Cont. Shelf Res. **43**: 71–85.
527 Mendez, J., C. Guieu, and J. Adkins. 2010. Atmospheric input of manganese and iron to the ocean:
528 Seawater dissolution experiments with Saharan and North American dusts. Mar. Chem.
529 **120**: 34–43. doi:10.1016/j.marchem.2008.08.006
530 Morgan, J. J. 2005. Kinetics of reaction between O2 and Mn(II) species in aqueous solutions.
531 Geochim. Cosmochim. Acta **69**: 35–48. doi:10.1016/j.gca.2004.06.013
532 Mottl, M. J., F. J. Sansone, C. Geoffrey Wheat, J. A. Resing, E. T. Baker, and J. E. Lupton. 1995.
533 Manganese and methane in hydrothermal plumes along the East Pacific Rise, 8°40′ to
534 11°50′N. Geochim. Cosmochim. Acta **59**: 4147–4165. doi:10.1016/0016-7037(95)00245-
535 U

Murray, J. W., B. Spell, and B. Paul. 1983. The contrasting geochemistry of manganese and chromium in the eastern tropical Pacific Ocean, p. 643–669. *In* Trace metals in sea water. Springer.

Oldham, V. E., M. R. Jones, B. M. Tebo, and G. W. Luther. 2017a. Oxidative and reductive processes contributing to manganese cycling at oxic-anoxic interfaces. Mar. Chem. **195**: 122–128. doi:10.1016/j.marchem.2017.06.002

Oldham, V. E., C. H. Lamborg, and C. M. Hansel. 2020. The Spatial and Temporal Variability of Mn Speciation in the Coastal Northwest Atlantic Ocean. J. Geophys. Res. Oceans **125**. doi:10.1029/2019JC015167

Oldham, V. E., A. Mucci, B. M. Tebo, and G. W. Luther. 2017b. Soluble Mn(III)–L complexes are abundant in oxygenated waters and stabilized by humic ligands. Geochim. Cosmochim. Acta **199**: 238–246. doi:10.1016/j.gca.2016.11.043

Perez-Benito, J. F. 2002. Reduction of Colloidal Manganese Dioxide by Manganese(II). J. Colloid Interface Sci. **248**: 130–135. doi:10.1006/jcis.2001.8145

Peters, B. D., W. J. Jenkins, J. H. Swift, C. R. German, J. W. Moffett, G. A. Cutter, M. A. Brzezinski, and K. L. Casciotti. 2018. Water mass analysis of the 2013 US GEOTRACES eastern Pacific zonal transect (GP16). Mar. Chem. **201**: 6–19. doi:10.1016/j.marchem.2017.09.007

Resing, J. A., P. N. Sedwick, C. R. German, W. J. Jenkins, J. W. Moffett, B. M. Sohst, and A. Tagliabue. 2015. Basin-scale transport of hydrothermal dissolved metals across the South Pacific Ocean. Nature **523**: 200–203. doi:10.1038/nature14577

Ruppel, D. T., S. C. Dexter, and G. W. Luther. 2001. Role of Manganese Dioxide in Corrosion in the Presence of Natural Biofilms. CORROSION **57**: 863–873. doi:10.5006/1.3290313

559 Rush, J. D., and B. H. J. Bielski. 1985. Pulse radiolytic studies of the reaction of
560 perhydroxyl/superoxide O2- with iron(II)/iron(III) ions. The reactivity of HO2/O2- with
561 ferric ions and its implication on the occurrence of the Haber-Weiss reaction. 5.
562 Sander, S. G., A. Koschinsky, G. Massoth, M. Stott, and K. A. Hunter. 2007. Organic complexation
563 of copper in deep-sea hydrothermal vent systems. Environ. Chem. **4**: 81–89.
564 doi:10.1071/EN06086
565 Sanial, V., L. E. Kipp, P. B. Henderson, and others. 2017. Radium-228 as a tracer of dissolved trace
566 element inputs from the Peruvian continental margin. Mar. Chem.
567 doi:10.1016/j.marchem.2017.05.008
568 Shaw, T. J., G. W. Luther, R. Rosas, and others. 2021. Fe-catalyzed sulfide oxidation in
569 hydrothermal plumes is a source of reactive oxygen species to the ocean. Proc. Natl. Acad.
570 Sci. **118**: e2026654118. doi:10.1073/pnas.2026654118
571 Stone, A. T. 1987. Reductive Dissolution of Manganese(III/Iv) Oxides by Substituted Phenols.
572 Environ. Sci. Technol. **21**: 979–988. doi:10.1021/es50001a011
573 Stone, A. T., and J. J. Morgan. 1984. Reduction and dissolution of manganese (III) and manganese
574 (IV) oxides by organics. 1. Reaction with hydroquinone. Environ. Sci. Technol. **18**: 450–
575 456.
576 Stumm, W., and J. J. Morgan. 1996. Aquatic chemistry: chemical equilibria and rates in natural
577 waters, John Wiley & Sons.
578 Sunda, W. G., and S. A. Huntsman. 1988. Effect of sunlight on redox cycles of manganese in the
579 southwestern Sargasso Sea. Deep Sea Res. Part Oceanogr. Res. Pap. **35**: 1297–1317.
580 doi:10.1016/0198-0149(88)90084-2

Sunda, W. G., and S. A. Huntsman. 1990. Diel cycles in microbial manganese oxidation and manganese redox speciation in coastal waters of the Bahama Islands. Limnol. Oceanogr. **35**: 325–338. doi:10.4319/lo.1990.35.2.0325

Sunda, W. G., S. A. Huntsman, and G. R. Harvey. 1983. Photoreduction of manganese oxides in seawater and its geochemical and biological implications. Nature **301**: 234–236. doi:10.1038/301234a0

Thibault de Chanvalon, A., and G. W. Luther. 2019. Mn speciation at nanomolar concentrations with a porphyrin competitive ligand and UV–vis measurements. Talanta **200**: 15–21. doi:10.1016/j.talanta.2019.02.069

Trouwborst, R. E., B. G. Clement, B. M. Tebo, B. T. Glazer, and G. W. Luther. 2006. Soluble Mn(III) in Suboxic Zones. Science **313**: 1955–1957. doi:10.1126/science.1132876

Van Cappellen, P., and Y. Wang. 1996. Cycling of iron and manganese in surface sediments; a general theory for the coupled transport and reaction of carbon, oxygen, nitrogen, sulfur, iron, and manganese. Am. J. Sci. **296**: 197–243.

Vedamati, J., C. Chan, and J. W. Moffett. 2015. Distribution of dissolved manganese in the Peruvian Upwelling and Oxygen Minimum Zone. Geochim. Cosmochim. Acta **156**: 222–240. doi:10.1016/j.gca.2014.10.026

Yakushev, E., S. Pakhomova, K. Sørenson, and J. Skei. 2009. Importance of the different manganese species in the formation of water column redox zones: Observations and modeling. Mar. Chem. **117**: 59–70. doi:10.1016/j.marchem.2009.09.007

Supporting Information

Supporting Information, Table S1: Dataset of Mn concentration and speciation.

NH_2OH reduced method was not processed on 4/13 and 4/15.

Date	Depth (m)	σ_θ	"heated only"method	"NH_2OH reduced" method	"HA removed" method	% Mn(III)-humic acid
April 4th	1	21.0	2.8 ± 0.5	3.6 ± 0.5	2.8 ± 0.5	- ± -
April 4th	30	21.4	2.9 ± 0.5	3.0 ± 0.4	3.1 ± 0.7	- ± -
April 4th	70	23.0	3.2 ± 0.6	3.7 ± 0.5	3.2 ± 1.5	- ± -
April 4th	85	24.8	5.4 ± 1	5.9 ± 1.9	5.6 ± 0.7	- ± -
April 4th	98	26.1	3.4 ± 0.4	3.5 ± 0.7	2.5 ± 0.5	- ± -
April 4th	260	27.7	2.7 ± 0.5	3.0 ± 0.5	2.1 ± 0.6	- ± -
April 4th	500	29.2	4.4 ± 0.9	4.6 ± 0.5	3.9 ± 0.6	- ± -
April 4th	615	29.9	4.1 ± 0.9	4.0 ± 0.4	3.3 ± 0.5	- ± -
April 4th	1400	34.1	2.8 ± 0.4	3.1 ± 0.6	2.4 ± 0.8	- ± -
April 4th	2000	37.0	2.5 ± 0.4	3.0 ± 0.4	2.7 ± 0.8	- ± -
April 4th	2494	39.3	28.2 ± 1.9	26.6 ± 1.4	10.2 ± 5.0	64.0 ± 19.0
April 6th	1	21.2	2.7 ± 0.2	2.8 ± 0.3	2.3 ± 0.3	- ± -
April 6th	30	21.4	2.6 ± 0.2	2.3 ± 0.3	2.3 ± 0.3	- ± -
April 6th	65	23.0	2.7 ± 0.2	2.6 ± 0.3	2.6 ± 0.3	- ± -
April 6th	70	23.9	3.7 ± 0.3	3.6 ± 0.4	3.7 ± 0.3	- ± -
April 6th	80	25.0	2.5 ± 0.3	2.2 ± 0.3	2.7 ± 0.4	- ± -
April 6th	90	25.6	2.9 ± 0.8	3.0 ± 0.3	3.3 ± 0.2	- ± -
April 6th	100	26.0	3.0 ± 0.3	2.4 ± 0.4	3.5 ± 0.3	- ± -
April 6th	110	26.4	3.0 ± 0.2	2.8 ± 0.3	3.4 ± 0.2	- ± -
April 6th	260	27.8	2.4 ± 0.6	2.0 ± 0.4	1.3 ± 0.5	- ± -
April 6th	400	28.6	3.7 ± 0.2	3.6 ± 0.3	3.3 ± 0.3	- ± -
April 6th	615	30.0	3.7 ± 0.4	3.2 ± 0.3	3.2 ± 0.5	- ± -
April 6th	1500	34.6	2.4 ± 0.2	3.0 ± 1.7	2.0 ± 0.5	- ± -
April 6th	2500	39.3	5.1 ± 0.4	5.8 ± 0.4	5.7 ± 0.3	- ± -
April 13th	30	21.2	5.1 ± 0.3		5.1 ± 0.6	- ± -
April 13th	60	22.1	4.9 ± 0.3		4.8 ± 0.4	- ± -
April 13th	73	23.4	8.4 ± 0.5		6.8 ± 0.5	19.3 ± 8.0
April 13th	80	24.4	5.3 ± 0.4		5.8 ± 0.6	- ± -
April 13th	86	26.9	5.3 ± 0.3		3.5 ± 0.3	33.5 ± 8.0
April 13th	140	27.9	14.2 ± 0.9		7.6 ± 0.8	46.6 ± 8.3

April 13th	400	28.9	8.2 ± 0.5	4.1 ± 1.5	49.7 ± 19.5
April 13th	530	29.9	5.5 ± 0.5	4.4 ± 0.4	20.0 ± 11.6
April 13th	700	30.9	3.6 ± 0.4	3.2 ± 0.3	- ± -
April 13th	1500	31.9	2.4 ± 0.4	2.7 ± 0.4	- ± -
April 13th	2000	32.9	3.5 ± 0.7	2.6 ± 0.4	- ± -
April 13th	2500	33.9	20.7 ± 1.1	12.5 ± 0.7	39.7 ± 6.0
April 15th	50	21.8	4.7 ± 1.1	4.5 ± 0.7	- ± -
April 15th	60	22.3	5.2 ± 0.9	3.7 ± 0.7	- ± -
April 15th	70	23.2	5.7 ± 0.5	3.5 ± 0.8	37.2 ± 17.1
April 15th	76	23.6	6.0 ± 0.4	3.1 ± 0.9	47.7 ± 16.1
April 15th	82.5	24.2	5.5 ± 0.6	4.1 ± 0.4	24.6 ± 13.2
April 15th	110	26.3	6.9 ± 0.5	4.7 ± 0.8	32.7 ± 12.9
April 15th	680	30.3	10.2 ± 1.4	8.1 ± 0.6	20.3 ± 15.3
April 15th	1500	34.6	2.2 ± 0.5	2.1 ± 0.6	- ± -
April 15th	2500	39.3	134.4 ± 7.5	85.1 ± 4.3	36.7 ± 6.4

605

606 **Supporting Information, Figure S1: Temperature and beam transmission in the**

607 **deeper meters from CTD casts.**

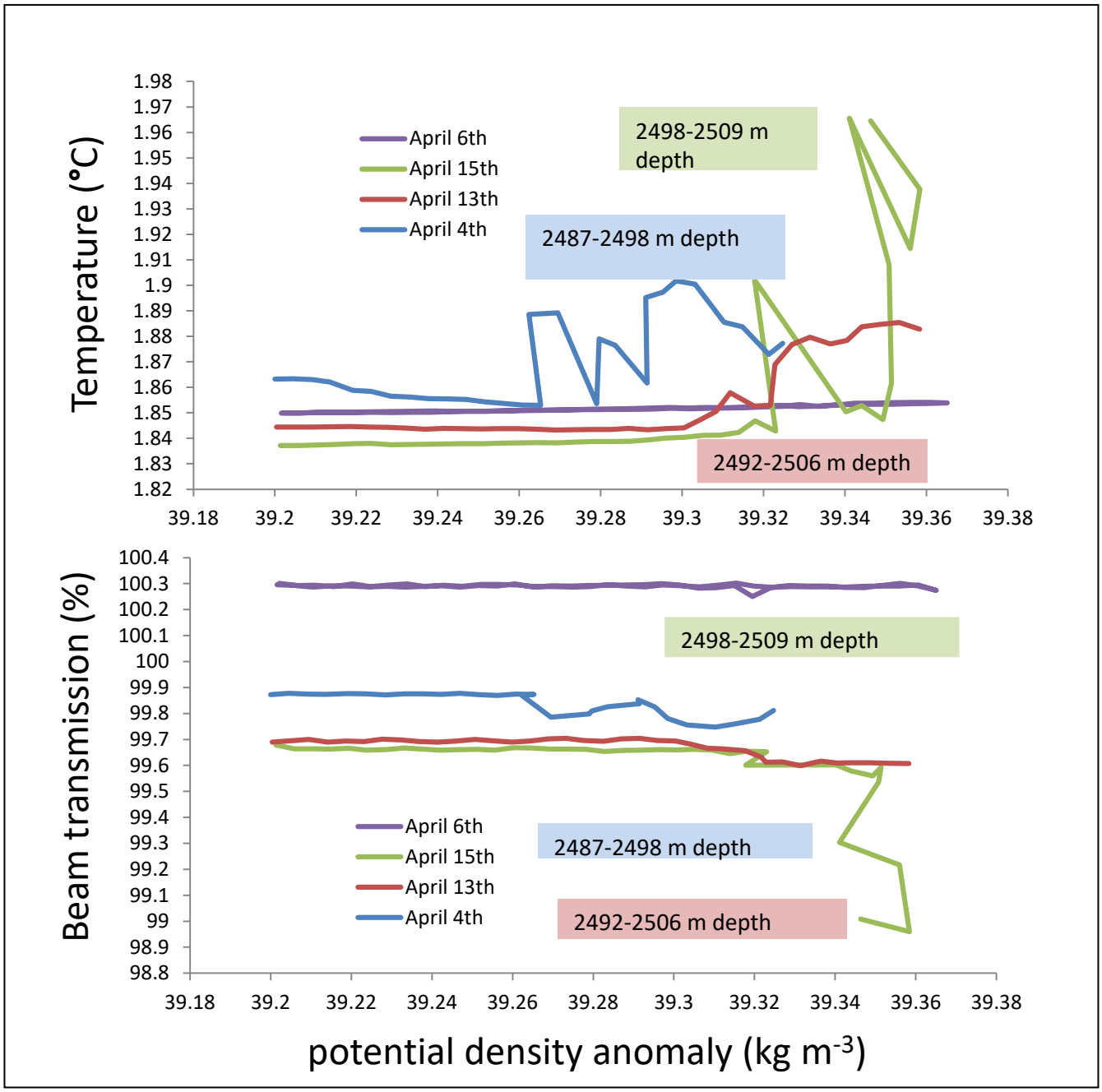

608